The interplay between molecular assembly and phase separation

Giacomo Bartolucci,[1,2] Thomas C.T. Michaels,[3] and Christoph A. Weber[4]

[1] *Max Planck Institute for the Physics of Complex Systems, Nöthnitzer Strasse 38, 01187 Dresden, Germany*
[2] *Center for Systems Biology Dresden, Pfotenhauerstrasse 108, 01307 Dresden, Germany*
[3] *ETH Zurich, Institute of Biochemistry, 8092, Zurich, Switzerland*
[4] *Faculty of Mathematics, Natural Sciences, and Materials Engineering: Institute of Physics, University of Augsburg, Universitätsstraße 1, 86159 Augsburg, Germany*

(Dated: April 19, 2023)

Interactions among proteins in living cells can lead to molecular assemblies of different sizes and large-scale coexisting phases formed via phase separation. Both are essential for the spatial organization of cells and for regulating biological function and dysfunction. A key challenge is understanding the interplay between molecular assembly and phase separation. However, a corresponding theoretical framework that relies on thermodynamic principles is lacking. Here, we present a non-equilibrium thermodynamic theory for a multi-component mixture that contains assemblies of different sizes, which can form, dissolve, and phase-separate from the solvent. We show that the size distributions of assemblies differ between the phases and that the dense phase can gelate. Moreover, we unravel the mechanisms involved in growth and compositional changes of the coexisting phases during assembly kinetics. Our theory can explain how molecular assembly is intertwined with phase separation, and our results are consistent with recent experimental observations on protein phase separation.

I. SIGNIFICANCE STATEMENT

Most biological functions and dysfunctions rely on two fundamental processes, molecular assembly and the formation of condensed phases such as biomolecular condensates. Condensed phases generally form via phase separation, while molecular assemblies are assemblies of molecules of various sizes, shapes, and functionality. We developed a theory that relies on thermodynamic principles to understand the interplay between molecular assembly and phase separation. We obtain results consistent with recent in vitro experimental observations of reconstituted proteins, including anomalous size distribution of assemblies and the gelation of condensed phases. Our theory provides the framework to unravel the mechanisms underlying physiological assemblies essential for cellular function, and aberrant assemblies that are associated with several neurodegenerative disorders.

II. INTRODUCTION

Due to their structural complexity, proteins can interact in different ways, leading to coexisting phases or assemblies such as fibers and aggregates. Long-lived assemblies are often kept together by strong adhesive forces, with corresponding binding free energies ranging from 9 k_BT in the case of insulin dimers [1], over 2.5 k_BT per beta sheet in amyloid fibers, to the 0.9 k_BT per beta-sheet in the formation of assemblies of specific FUS segments called low-complexity aromatic-rich kinked segments [2]. Weak interactions are often responsible for the separation into liquid phases, each of distinct molecular compositions. The interaction free energies associated with the formation of P granules via phase separation in living cells are about 0.5 k_BT per molecule [3]. The biological function of both assemblies and phase-separated compartments relies on the recruitment of specific biomolecules such as proteins, RNA or DNA [4–7]. Since assemblies and condensed phases can adhere to membrane surfaces, both not only mediate mechanisms for sorting and transport of molecules [8] but also affect the composition, shape and properties of intra-cellular surfaces [9–12].

Despite these similarities, molecular assemblies and coexisting phases also exhibit crucial differences. While the size of a condensed phase at equilibrium increases with the size of the system [13], this is not necessarily the case for molecular assemblies [14–16]. Moreover, the assembly kinetics tends to an equilibrium characterised by assemblies of different sizes [14–16], while condensed phases equilibrate the physio-chemical properties such as temperature, pressure and chemical potential between the spatially separated phases [13]. These differences suggest a rich interplay in a system where the molecular constituents can both oligomerise forming assemblies and give rise to coexisting phases [17–22].

In the last years, the interplay between phase separation and assembly formation has been the focus of many experimental efforts. Different proteins capable of forming condensed phases were shown to form oligomers below the saturation concentration [23, 24]. Moreover, different proteins capable of forming condensed phases were shown to form oligomers below the saturation concentration [23, 24]. The authors proposed that such oligomers affect the phase separation propensity, however, the detailed mechanism remains elusive. Moreover, several experimental studies of protein phase separation indicate that proteins in the dense phase are linked, reminiscent of a physical gel [25–27]. Molecular simulations were per-

formed that aimed at the sequence-specific origin of such phenomena [28–31]. However, even in elegantly coarse-grained simulation approaches, the large number of parameters makes it difficult to extract the general, mechanisms across different proteins. To develop an understanding of such general mechanisms that underlie the interplay between phase separation and molecular assembly, a theoretical framework that relies on thermodynamic principles is lacking.

While the theory of phase separation of a low number of different components [13, 32], as well as the formation of molecular assemblies in dilute environments [14, 33, 34], are well developed, only a few works addressed assembly formation beyond the dilute limit, where assemblies can form and also phase separate. For example, it has been shown that, in the presence of coexisting phases, the assembly size distributions at equilibrium can vary in the two phases and that the dense phase can gelate [35–38]. These studies account for the scaling of the internal free energies of assemblies with their size but neglect the size dependence of the interaction propensities. Moreover, a discussion of the coupled phase separation and assembly kinetics is lacking. Other authors focused on systems composed of a scaffold component, that drives phase separation, and study the dilute assembly kinetics of a second component that can interact with the scaffold [39–42]. In these works, the assemblies are considered to be dilute and the feedback of the assembly kinetics on the phase-separated compartment is neglected.

In this work, we introduce a framework that unifies the thermodynamic theories for phase separation with the theories developed for the formation of micelles and molecular assemblies at dilute conditions. We introduce two classes of size-dependent interactions that are inspired by biologically relevant proteins. We discuss the emergence of anomalous size distribution below saturation and the gelation of condensed phases above saturation, and characterise for which class and parameter values these phenomena manifest. Furthermore, we propose a non-equilibrium thermodynamic theory for the kinetics of molecular assembly at non-dilute conditions which can lead to macroscopic, condensed phases above the saturation concentration. The complexity of our theory is reflected in a high dimensional phase space that is set by the number of differently sized assemblies. We developed efficient numerical schemes to study the kinetics of such systems for the case where diffusion is fast compared to assembly kinetics. We could thus identify various properties of molecular assemblies that distinctly originate from non-dilute conditions. Our theory could be key to interpreting and understanding recent observations of protein condensation in vitro [43], in the cell cytoplasm [24, 27, 44, 45].

III. ASSEMBLY AND PHASE EQUILIBRIA

We begin by reviewing the equilibrium theory of multi-component mixtures composed of solvent (s) and monomers ($i = 1$) that can form assemblies composed of i monomers, see Fig. 1a. In the case when monomers and assemblies are dissolved in the solvent, the free energy density of the solution can be written as [35, 37, 46, 47]:

$$f_{\rm sol} = \frac{k_B T}{\nu_{\rm s}} \left(\sum_{i=1}^{M} \frac{\phi_i}{\rho_i} \ln\left(\frac{\phi_i}{\rho_i}\right) + \frac{\omega_i}{k_B T}\phi_i + \sum_{i\neq j=1}^{M} \frac{\chi_{ij}}{2k_B T}\,\phi_i\phi_j + \phi_{\rm s}\ln\phi_{\rm s} + \frac{\omega_{\rm s}}{k_B T}\phi_{\rm s} + \sum_{i=1}^{M} \frac{\chi_{i{\rm s}}}{k_B T}\,\phi_i\phi_{\rm s} \right), \tag{1}$$

where $\rho_i = \nu_i/\nu_{\rm s}$ are the relative molecular volumes, ν_i is the molecular volume of assembly of size i, and $\nu_{\rm s}$ is the solvent molecular volume. The solvent volume fraction can be expressed as a function of the assembly volume fractions via $\phi_{\rm s} = 1 - \sum_{i=1}^{M} \phi_i$. The first and fourth terms in Eq. (1) are the mixing entropies. The second and fifth terms of $f_{\rm sol}$ characterize the internal free energies. Here, $\omega_{\rm s}$ denotes the internal free energy of the solvent, and ω_i are the internal free energies per monomer of an assembly of size i. Note that we chose to keep ϕ_i/i in the logarithm argument instead of reabsorbing the linear term $-\phi_i \ln(i)/i$ in the internal free energies ω_i. With this choice, ω_i, depends only on bond free energies, see App. A, Ref. [46], and the recent overview in the SI of Ref. [41]. The third and last terms in Eq. (1) capture the interactions of monomers belonging to different assemblies and with the solvent, where χ_{ij} is the corresponding interaction parameter. The exchange chemical potentials of monomers belonging to an assembly of size i reads

$$\mu_i = \nu_1 \frac{\partial f_{\rm sol}}{\partial \phi_i}\,. \tag{2}$$

Assembly equilibrium. Assemblies can grow and shrink via association and dissociation. Such transitions among assemblies of different sizes are reminiscent of chemical transitions, see Fig. 1a. The condition of chemical equilibrium reads [16]:

$$\mu_i = \mu_1 = \text{const.} \quad \forall\, i = 2 \ldots M\,, \tag{3}$$

where μ_i is the exchange chemical potential of monomers belonging to an assembly of size i; see Eq. (2). Using the free energy Eq. (1) and the equilibrium conditions Eq. (3), we can express the volume fraction of the assembly of size i as a function of the monomer volume fraction ϕ_1 in the following form:

$$\phi_i = \rho_i \left(\frac{\phi_1}{\rho_1}\right)^{\rho_i/\rho_1} \exp\left[r_i \left(1 - \frac{\omega_i - \omega_1}{k_B T} - \frac{\chi_{i{\rm s}} - \chi_{1{\rm s}}}{k_B T}\phi_{\rm s} - \sum_j \frac{\chi_{ij} - \chi_{1j}}{k_B T}\phi_j \right) - 1 \right]. \tag{4}$$

The equation above together with the conservation of monomers

$$\phi_{\rm tot} = \sum_{i=1}^{M} \phi_i \,, \tag{5}$$

allows us to rewrite the volume fraction ϕ_i of each assembly of size i, as a function of the conserved quantity $\phi_{\rm tot}$. This relation $\phi_i = \phi_i(\phi_{\rm tot})$ has an analytical expression in the case $d = 1$, see Eq. (B1) and Eq. (B3) in SI B.

Phase equilibrium. Two phases in an incompressible, multi-component system are at phase equilibrium when the chemical potentials μ_i and the osmotic pressure $\Pi = -f_{\rm sol} + \sum_{i=1}^{M} \phi_i \partial f_{\rm sol}/\partial \phi_i$ balance in each phase [13, 48]:

$$\mu_i^{\rm I} = \mu_i^{\rm II} \,, \tag{6a}$$

$$\Pi^{\rm I} = \Pi^{\rm II} \tag{6b}$$

where the superscripts I and II indicate the $\phi_{\rm tot}$-rich and II the $\phi_{\rm tot}$-poor phase, respectively. *Thermodynamic equilibrium.* Our system is at thermodynamic equilibrium when assembly and phase equilibrium hold simultaneously. The conditions above for phase equilibrium can thus be rewritten using $\phi_i\,(\phi_{\rm tot})$ (Eq. (4)). In particular, the free energy density Eq. (1) can be recasted in terms of the conserved variable, $\phi_{\rm tot}$ [49, 50]. The phase diagram of the system can be then obtained via the common tangent construction (i.e., Maxwell construction). This construction corresponds to the balance between the exchange chemical potentials and the osmotic pressure in both phases, see Chapter 2 in Ref. [49, 50]:

$$\mu(\phi_{\rm tot}^{\rm I}) = \mu(\phi_{\rm tot}^{\rm II}) \,, \tag{7a}$$

$$\mu(\phi_{\rm tot}^{\rm I}) = \frac{f_{\rm sol}(\phi_{\rm tot}^{\rm II}) - f_{\rm sol}(\phi_{\rm tot}^{\rm I})}{\phi_{\rm tot}^{\rm II} - \phi_{\rm tot}^{\rm I}} \,. \tag{7b}$$

IV. SCALING OF MOLECULAR VOLUMES, INTERNAL FREE ENERGIES AND INTERACTION ENERGIES WITH ASSEMBLY SIZE

The composition of the phase-separated compartments and the size distributions of the assemblies in each phase will depend on the scaling form of the key parameters of the model: the relative molecular volumes (r_i), the internal free energy of assemblies (ω_i), and the interaction energies of assemblies among themselves (χ_{ij}), and with the solvent (χ_{is}). For simplicity, we choose $r_i = i$ for the results shown in this work. In Appendix A, we derive the scaling relationships for the internal free energies of rod-like ($d = 1$), disk-like ($d = 2$) and spherical ($d = 3$) assemblies:

$$\omega_i \simeq \omega_\infty - \frac{e_{\rm int} - s_{\rm int} T}{i^{1/d}} \,. \tag{8}$$

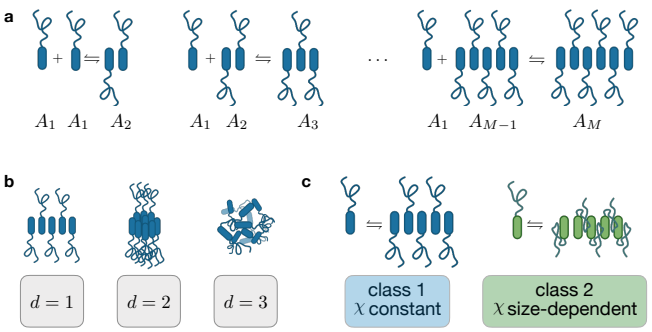

FIG. 1. **Illustration of assembly reaction scheme and classification**. **a** Illustration of the chemical reaction network associated with the formation of assemblies A_i with size i, in the special case where growth and shrinkage occur only via monomer pick-up and release. **b** Identification of three classes based on assembly dimension: d=1,2,3. **c** Classification of assemblies based on the scaling of their Flory-Huggins interaction propensity.

Here, $\omega_\infty = \lim_{i\to\infty} \omega_i$ is a constant that does not affect chemical nor phase equilibrium, except in the limit $M \to \infty$, which will be discussed later. Moreover, $e_{\rm int} - s_{\rm int} T$, is the free energy of an internal bond that keeps each assembly together, which can be separated into an enthalpic and an entropic contribution, $e_{\rm int}$ and $s_{\rm int}$, respectively.

For the scaling of interaction energies χ_{ij} and χ_{is}, we introduce two classes inspired by biologically relevant classes of proteins that can form assemblies and phase separate:

1. **Class 1: Constant assembly-solvent interactions.**
   This class corresponds to the case where each monomer, independently of the assembly it is part of, interacts equally with the solvent $\chi_{is} = \chi$, see App. A. Moreover, monomers in assemblies of different sizes interact equally with each other, implying that the corresponding Flory-Huggins parameter χ_{ij} vanishes:

   $$\chi_{is} = \chi \,, \qquad \chi_{ij} = 0 \,. \tag{9}$$

   This class is inspired by biologically relevant proteins for which the oligomerization domains are well separated along the protein from hydrophobic phase separation domains. In this case, when monomers form an assembly, their phase separation domains remain exposed, leading to a monomer-solvent interaction that does not depend on assembly size. Examples belonging to this class include synthetic constructs like the so-called 'Corelets' [51], realised tethering intrinsically disordered protein fragments to oligomerizing domains [51], and proteins like NPM1, whose N-terminal oligomerization domain (that allows for the formation of pentamers) is considered to be

separated from the disordered region (responsible for phase separation) and the RNA binding domain [52, 53].

2. **Class 2: Size-dependent assembly-solvent interactions.** This class describes the case where monomers in the assembly bulk and monomers at the assembly boundary have different interaction propensities with the solvent (χ' and χ respectively, see Appendix A for details). Similar to class 1, monomers in assemblies of different sizes interact equally with each other, leading to

$$\chi_{is} = \chi' + \frac{\chi - \chi'}{i^{1/d}}\,, \quad \chi_{ij} = 0\,. \tag{10}$$

This class corresponds to the general case in which the oligomerization domains of protein overlap with the phase separation domains. This case applies to segments of the intrinsically disordered region of the protein FUS, for example. In fact, recent experiments have shown the formation of assemblies in solutions containing specific FUS domains, called low-complexity aromatic-rich kinked segments (LARKS) [2, 54]. Strikingly, it was shown that hydrophobic domains along LARKS were buried in the formation of these assemblies and the author could quantify the hydrophobic area buried upon assembly formation. Another example could be Whi3, since it has been recently found that mutation that enhances oligomerization strength, lowers the density of Whi3 in the RNP condensates [45], suggesting that the formation of assemblies could screen Whi3 phase separation propensity.

V. ASSEMBLY SIZE DISTRIBUTIONS BELOW AND ABOVE SATURATION

We first consider systems that are spatially homogeneous and composed of linear assemblies ($d = 1$). Homogeneity can be realized in dilute solutions if the total protein volume fraction $\phi_{\rm tot}$ lies below the saturation concentration of phase separation $\phi^{\rm II}_{\rm tot}(T)$ (definition see Section III). Homogeneous systems governed by Eq. (4) at equilibrium and the conservation Eq. (5) exhibit two limiting behaviours depending on the value of the conserved variable $\phi_{\rm tot}$. We define the *assembly threshold* $\phi^*(T)$, that separates these two behaviours as the value of $\phi_{\rm tot}$ (see Eq. (5)) for which the distribution ϕ_i has a maximum corresponding to monomers:

$$\frac{\partial \phi_i}{\partial i}\Big|_{i_{\rm max}} = 0, \quad i_{\rm max}(\phi^*) = 1\,. \tag{11}$$

Indeed, for $\phi_{\rm tot} \ll \phi^*$ the size distribution of linear assemblies ($d = 1$) is dominated by monomers ($\phi_1 \simeq \phi_{\rm tot}$) while larger assemblies have vanishing volume fraction. For higher volume total volume fractions ($\phi_{\rm tot} \gtrsim \phi^*$), the monomer concentration saturates at $\phi_1 \lesssim \phi^*$ and bigger assemblies start to populate the mixture. Above ϕ^*, the distribution becomes peaked at a value $i_{\rm max} > 1$ and then exponentially decays for larger i; see App. Fig. 6. Both the maximum and the average of the distribution ϕ_i scale with $\sqrt{\phi_{\rm tot}}$ indicating that as $\phi_{\rm tot}$ is increased larger and larger assembly populate the system; see Appendix B for a detailed discussion for Class 1.

Now we consider systems that can phase separate. As outlined in Sec. III, at assembly equilibrium, we can recast the free energy as a function of the conserved variable $\phi_{\rm tot}$ by using Eq. (4). For sufficiently large assembly-solvent interaction parameters χ and χ', the system can demix into two phases with different total volume fractions $\phi^{\rm I}_{\rm tot}$ and $\phi^{\rm II}_{\rm tot}$, which are the solutions of Eq. (7). By means of $\phi^{\rm I/I}_{\rm tot}$, we can calculate the whole assembly size distribution in the two phases, i.e., $\phi_i^{\rm I/II}$, via Eq. (4) and Eq. (5).

We first discuss linear assemblies belonging to class 1, in the regime of high assembly strength $-e_{\rm int}/\chi \gg 1$; see Fig. 2a-c. In Fig. 2a, we show the corresponding phase diagram as a function of $\phi_{\rm tot}$ and the rescaled temperature T/T_0 with $T_0 = \chi/k_B$. The domain enclosed by the binodal corresponds to phase separation. As indicated by the colour code (depicting the monomer fraction $\phi_1/\phi_{\rm tot}$) each phase can have different assembly composition. In green we plot the assembly threshold $\phi^*(T)$, at which intermediate-sized assemblies start to appear. Note that, with this choice of parameters, the assembly threshold precedes in $\phi_{\rm tot}$ the dilute branch of the binodal. We can thus define regions corresponding to qualitatively different phase and assembly behaviours. In particular, starting from a homogeneous system composed of monomers only (region "i"), increasing $\phi_{\rm tot}$ leads to the emergence of intermediate-sized assemblies (region "ii"). Increasing $\phi_{\rm tot}$ further, the system demixes into two phases both of which are rich in intermediate assemblies (region "iii"). Representative size distributions and illustrations of the state of the systems in the different regions are shown in Fig. 2b and Fig. 2c, respectively. This analysis showcases the potential of this framework to describe the appearance of mesoscopic clusters below the saturation concentration, as recently observed experimentally in Ref. [24].

Remaining within class 1, we now discuss the case of low assembly strength $-e_{\rm int}/\chi \sim$; see Fig. 2d-f. The interception between the binodal and the assembly threshold ϕ^* defines two new regions, "iv" and "v", see Fig 2 d. In particular, in region "iv" both binodal branches lie below the assembly threshold, resulting in monomers dominating both coexisting phases, see Fig 2e, centre. On the other hand, in region "iv" the dense phase exceeds the assembly threshold, resulting in phases with different compositions: the dilute phase is populated only by monomers while intermediate-sized assemblies develop in the dense phase, see Fig 2e right. In Fig 2f, we illustrate states corresponding to fixed $\phi_{\rm tot}$ and decreasing temperature T. Starting from a homogeneous monomeric state, region "i", the system transitions into a demixed state

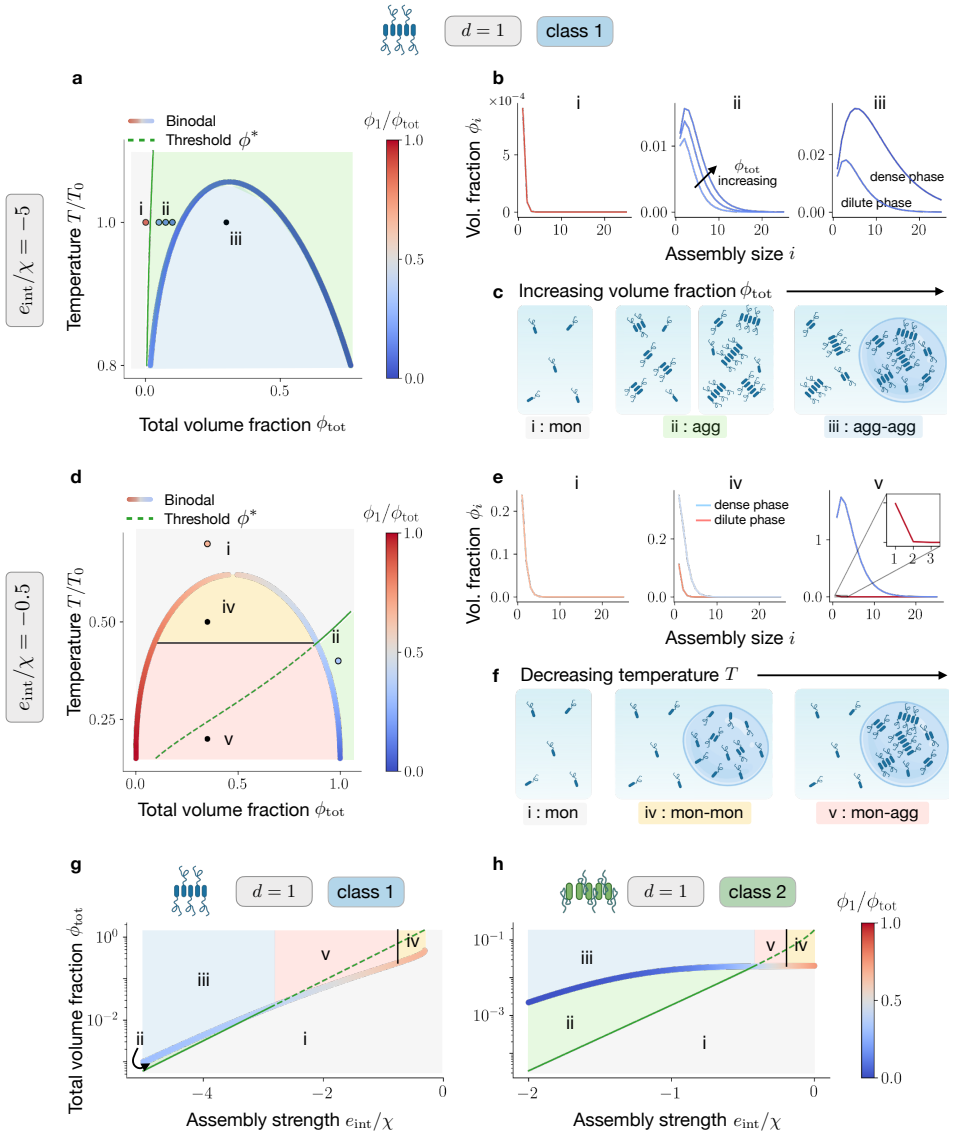

FIG. 2. **Phase diagram and assembly size distributions for different classes and assembly strengths. a** Phase diagram as a function of $\phi_{\rm tot}$ and rescaled temperature T/T_0 (with $T_0 = \chi/k_B$) in the regime of high assembly strength, i.e. $-e_{\rm int}/\chi \gg 1$. The green line is the volume fraction threshold $\phi^*(T)$ at which intermediate-sized assemblies start to appear, which in this regime precedes the binodal (coloured curve). As indicated by the colour code, the monomer fraction $\phi_1/\phi_{\rm tot}$ mildly varies in the two phases. **b** Size distributions and **c** pictorial representations corresponding to different regions of the phase diagram, defined by the relative position of the binodal and the assembly threshold. In region "i", the system is homogeneous and composed of monomers only. Increasing the total volume fraction of assemblies $\phi_{\rm tot}$ beyond the assembly threshold ϕ^*, the system enters region "ii" where intermediate assemblies appear. Here, the sizes corresponding to the maximum and the average of the distribution ϕ_i scale with $\sqrt{\phi_{\rm tot}}$, see Appendix B. Finally, once $\phi_{\rm tot}$ exceeds the binodal, the system enters region "v" and demixes in two phases, both rich in intermediate assemblies. In **d-f** we focus on the low assembly strength regime, i.e. $-e_{\rm int}/\chi \sim 1$. In phase diagram **d**, the binodal now precedes in $\phi_{\rm tot}$ the assembly threshold. **e** In region "iv", the system phase separates but in both phases monomers dominate the size distribution, while in region "v" the dense phase becomes populated by intermediate-sized assemblies. Progressively lowering the temperature allows switching between these regions, as depicted in **f**. **g,h** Behaviour of dilute mixtures as a function of assembly strength, for the two different classes. Notably, assembly below saturation becomes much more accessible for class 2, as can be seen by comparing the green regions "ii" in **g** and **h**.

with the same composition, region "iv", and finally to a demixed state with monomers only in one phase and larger assemblies in the other, region "v".

We now highlight the differences between the two classes defined in Sec. IV. In particular, we characterise how mixtures behave with increasing $\phi_{\rm tot}$, varying the assembly strength $e_{\rm int}/\chi$ but keeping the temperature T fixed. In particular, for class 1, the emergence of assem-

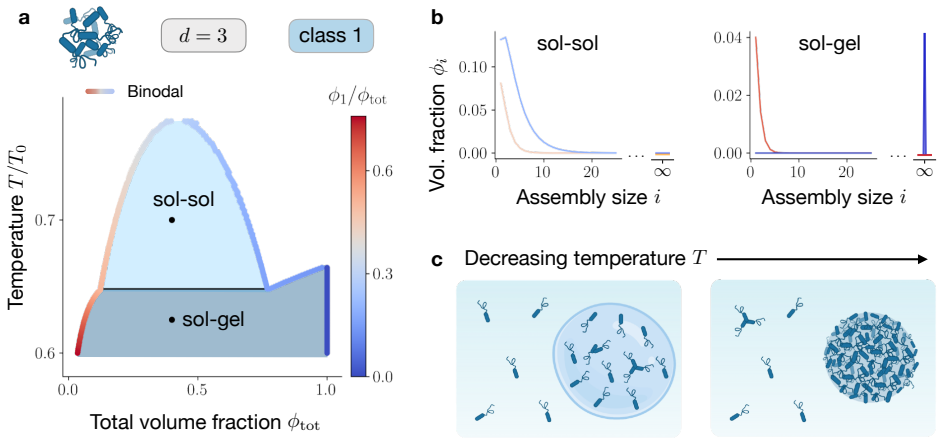

FIG. 3. **Gelation transition in phase-separating systems**. **a** Phase diagram for disk-like (d=2) and spherical (d=3) assemblies in the limit $M \to \infty$, as a function of $\phi_{\rm tot}$ and the rescaled temperature T/T_0 (with $T_0 = \chi/k_B$). The coloured curve represents the binodal associated with the free energy f, which accounts for the emergence of an infinite assembly. The colour code of the binodal line depicts the monomer fraction $\phi_1/\phi_{\rm tot}$ in the phases. In the region labelled as "sol-sol", the system demixes into two phases both populated mainly by monomers, see panel **b**, with $\phi_{\rm tot}^{\rm I/II} < 1$. In the region labelled as "sol-gel", on the other hand, a phase (the "sol"), obeying $\phi_{\rm tot}^{\rm sol} < 1$, coexists with a phase (the "gel") that is a macroscopic assembly, containing no solvent ($\phi_{\rm tot}^{\rm sol} = 1$). The latter scenario is represented in panel **b**, right side. **c** Lowering the temperature allows transitions from the "sol-sol" to the "sol-gel" region, which manifest with a jump in the total volume fraction of the dense phase.

blies before saturation typically occurs for a very narrow interval of volume fractions, see the green region labelled with "ii" in Fig 2g. Strikingly, for class 2, assembly below saturation are more favoured; see again region "ii" in Fig 2h. This difference arises because, within class 2, monomers in the bulk of an assembly have reduced interaction propensity with respect to the boundary ones. As a consequence, the formation of large clusters shifts the onset of phase separation to higher $\phi_{\rm tot}$ values.

VI. GELATION OF THE DENSE PHASE

Here, we discuss the case of disk-like ($d = 2$) and spherical assemblies, ($d = 3$), referring for simplicity to systems belonging to Class 1. In this case, as shown in App. C, even when neglecting protein solvent interactions ($\chi = 0$), the system can undergo a phase transition in the thermodynamic limit $M \to \infty$. In fact, above the volume fraction $\phi^{\rm sg}$ (for a definition see Eq. (C2)), we observe the emergence of a macroscopic assembly occupying a finite fraction of the system volume that contains a macroscopic fraction of all monomers in the system; a behaviour reminiscent of Bose-Einstein condensation, see for example Chapter 7.3 of Ref [37]. Since we do not explicitly include the solvent in assembly formation (see reaction scheme in Fig. 1a), we will consider the gel as a phase without solvent and thus $\phi_{\rm tot} = 1$.

We now focus on systems that phase separate as the result of interactions with the solvent ($\chi \neq 0$) and discuss the interplay with gelation. Volume fractions in the coexisting phases are determined by Eq. (7) and assembly equilibrium requires that Eq. (3) is satisfied. As pointed out in Sect. III, we aim to find an expression for $\phi_i(\phi_{\rm tot})$ via Eq. (3) and Eq. (5), and then substitute it into the free energy Eq. (1). However, for disk-like ($d = 2$) and spherical assemblies, ($d = 3$), performing the thermodynamic limit $M \to \infty$ leads to a free energy composed of series that cannot be analytically calculated. We know that this is a consequence of the gelation transition, and this limitation can be dealt with by introducing explicitly the infinite-sized gel in the free energy. For this reason, we write the system free energy as a composition of the solvent free energy $f_{\rm sol}$ and the gel free energy $f_{\rm gel}$:

$$f = f_{\rm sol} + f_{\rm gel}\,, \tag{12}$$

where $f_{\rm sol}$ is defined in Eq. (1). The gel free energy reads

$$f_{\rm gel} = \frac{\omega_\infty}{v_0}\,\delta\left(1 - \phi_{\rm tot}\right)\,, \tag{13}$$

with $\delta(\cdot)$ denoting the delta distribution. The gel free energy $f_{\rm gel}$ is the free energy of a state with no solvent, where all monomers belong to an assembly of size $i \to \infty$. In fact, in the limit $\phi_i = 0$ for all finite i and $\phi_{\rm tot} = 1$, the free energy in Eq. (1) simplifies to ω_∞/v_0. For a detailed discussion of the role of ω_∞, see App. C

We can now perform a Maxwell construction by using Eq. (12) in Eq. (7). The resulting phase diagram is displayed in Fig. 3a, where the binodal is coloured by the monomer fraction $\phi_1/\phi_{\rm tot}$ in the coexisting phases.

In phase-separated systems, gelation can be considered as a special case of phase coexistence between a dilute phase ("sol"), in which $\phi^{\rm sol} < 1$, and the gel phase, corresponding to $\phi^{\rm gel} = 1$. The domain in the phase diagram

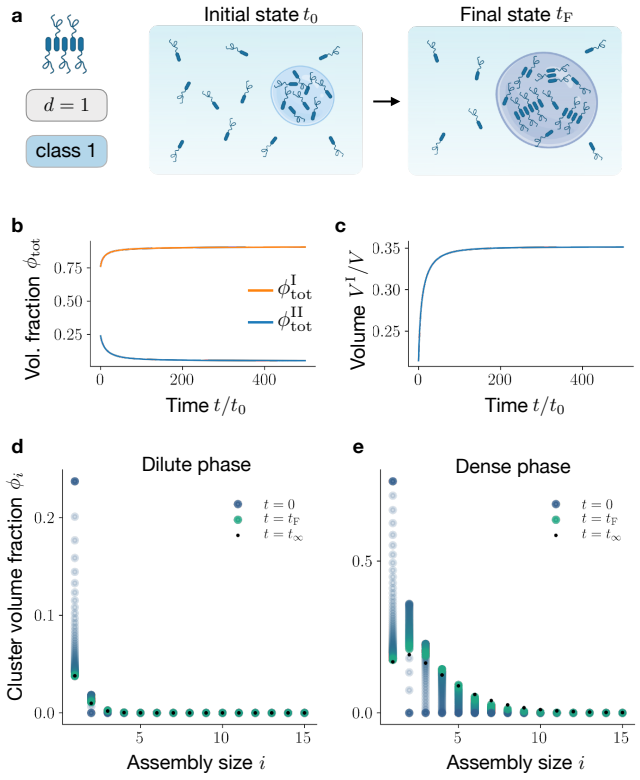

FIG. 4. **Assembly kinetics at phase equilibrium**. Assuming that the relaxation to phase equilibrium is fast compared to assembly kinetics, we study the slow relaxation to assembly equilibrium in a compartmentalized system. **a** In the sketch, assemblies selectively appear in the dense phase, increasing its volume $V^{\rm I}$ and total volume fraction $\phi_{\rm tot}^{\rm I}$. **b** As time proceeds, phase volumes change. This is reminiscent of recent experimental findings that quantify droplet volume changes along with droplet ageing [55]. **c** the total macromolecule volume fraction in the two phases, $\phi_{\rm tot}^{\rm I/II}$, changes in time. In particular, the $\phi_{\rm tot}$-dense phase becomes denser and the dilute phase more dilute. In **d** and **e** we show the time evolution of the full size distribution in the dilute and dense phases, respectively, starting from an initial state composed of monomers and solvent only.

where a gel phase coexists with a soluble phase is shaded in blue and labelled as "sol-gel" in Fig. 3a. In the same panel, we show that lowering the temperature for large $\phi_{\rm tot}$ leads to a transition from the homogeneous state to the sol-gel coexistence. By contrast, for intermediate volume fractions, the system transits first through a domain corresponding to two-phase coexistence; see light blue domain labelled as "sol-sol" in Fig. 3a, where $\phi_{\rm tot} < 1$ in both phases. In Fig. 3b, we show assembly size distributions representative of the "sol-sol" and "sol-gel" regions. The transition from the "sol-sol" to the "sol-gel" region is accompanied by a jump in the dense phase total volume fraction $\phi_{\rm tot}^{\rm I}$, see Fig. 3c for an illustration.

VII. KINETIC THEORY OF ASSEMBLY AT PHASE EQUILIBRIUM

Building upon the thermodynamic framework developed in the previous sections, we devise a non-equilibrium kinetic theory for molecular assembly at non-dilute conditions, where the interactions can give rise to coexisting phases. Here, we restrict ourselves to the case where each phase is homogeneous and at phase equilibrium but not at assembly equilibrium [56]; see Sect. III for the equilibrium conditions. This partial equilibrium holds when the molecular transitions among assemblies are slow compared to phase separation, i.e., the system is reaction-limited [57, 58]. This limit applies particularly well to molecular assemblies involving biological enzymes [59]. For simplicity, we present the kinetic theory and discuss the results for two coexisting phases. Following the concepts developed in Ref. [56], in each phase, the kinetics of the respective volume fractions of the assembly of size i, $\phi_i^{\rm I/II}$ for $i = 1, 2, ..., M$, is governed by

$$\frac{d}{dt}\phi_i^{\rm I/II} = r_i^{\rm I/II} - j_i^{\rm I/II} - \frac{\phi_i^{\rm I/II}}{V^{\rm I/II}}\frac{d}{dt}V^{\rm I/II}\,, \tag{14}$$

where $r_k^{\rm I/II}$ are the assembly rates in the corresponding phases of volumes $V^{\rm I/II}$, and $j_k^{\rm I/II}$ are the diffusive exchange rates between phases. The last term in Eq. (14) accounts for variations in volume fractions due to the changes of the respective phase volumes $V^{\rm I/II}$. The kinetics of phase volumes follow $(d/dt)\ln V^{\rm I/II} = \sum_{i=1}^{M} i(r_i^{\rm I/II} - j_i^{\rm I/II})$. In both phases, the solvent volume fraction can be expressed as $\phi_{\rm s}^{\rm I/II} = 1 - \phi_{\rm tot}^{\rm I/II}$, where

$$\phi_{\rm tot}^{\rm I/II} = \sum_{i=1}^{M} \phi_i^{\rm I/II} \tag{15}$$

is the total volume fraction of all assemblies. Consistently, assembly kinetics conserves $\phi_{\rm tot}$ in both phases. As a result, the assembly rates satisfy, $\sum_{i=1}^{M} r_i^{\rm I/II} = 0$ in each phase, leading to the simplified kinetic equation for compartment volume

$$\frac{d}{dt}\ln V^{\rm I/II} = -\sum_{i=1}^{M} j_i^{\rm I/II}\,. \tag{16}$$

Moreover, volume conservation also implies that the exchange currents fulfil

$$j_i^{\rm I} = -j_i^{\rm II}\frac{V^{\rm II}}{V^{\rm I}}\,. \tag{17}$$

This condition makes sure that the volume dynamics obey $(d/dt)(V^{\rm I} + V^{\rm II}) = 0$. The currents are determined by the conditions that maintain phase equilibrium, $d\mu_i^{\rm I}/dt = d\mu_i^{\rm II}/dt$ together with $d\Pi^{\rm I}/dt = d\Pi^{\rm II}/dt$, where $\mu_i^{\rm I/II}$ denote the chemical potentials of the monomers in

an assembly of size i, and Π the osmotic pressure; for more information, see SI F.

Utilizing our kinetic theory, we can study the relaxation toward thermodynamic equilibrium which corresponds to phase and assembly equilibrium. Here, we focus on assembly growth and shrinkage occurring via monomer pick-up and release, see reaction scheme in Fig. 1. However, note that our framework can be easily generalised to include other assembly mechanisms, including primary and secondary nucleation, association, and dissociation [60]. With these assumptions, the phase-dependent assembly rates for monomer exchange between assemblies of sizes i and $i+1$ are related to the chemical potentials via

$$r_{i+1,i} = k_i \left[\exp\left(\frac{i\,\mu_i + \mu_1}{k_B T} \right) - \exp\left((i+1) \frac{\mu_{i+1}}{k_B T} \right) \right] , \tag{18}$$

where k_i is a size-dependent rate coefficient. The monomer exchange rate $r_{i,i+1}$ determines the assembly rates of each assembly i via

$$\begin{aligned} r_1^{\mathrm{I/II}} &= -r_{2,1}^{\mathrm{I/II}} - \sum_{i=1}^{M-1} i\, r_{i+1,i}^{\mathrm{I/II}} , \\ r_i^{\mathrm{I/II}} &= (i-1)\, r_{i,i-1}^{\mathrm{I/II}} - i\, r_{i+1,i}^{\mathrm{I/II}} , \text{ for } i = 2, ..M-1 , \\ r_M^{\mathrm{I/II}} &= (M-1)\, r_{M,M-1}^{\mathrm{I/II}} . \end{aligned} \tag{19}$$

VIII. ASSEMBLY KINETICS IN COEXISTING PHASES

By integrating Eq. (14) numerically, we obtain the time evolution of $\phi_i^{\mathrm{I/II}}(t)$ and $V^{\mathrm{I}}(t)$, provided their initial values at $t = 0$, $V^{\mathrm{I}}(t=0)/V$, and $\phi_i^{\mathrm{I/II}}(t=0)$, at phase equilibrium. Specifically, we consider an initial state solely composed of solvent and monomers which are separated from each other and we focus on linear assemblies ($d = 1$) belonging to class 1; for parameters see caption of Fig. 4. As monomers begin to form assemblies, the mixing entropy decreases. As a result, the total amount of protein in the monomer-rich phase, $\phi_{\mathrm{tot}}^{\mathrm{I}}$, increases while $\phi_{\mathrm{tot}}^{\mathrm{II}}$ decreases (Fig. 4b). Such changes in total protein volume fractions induce phase volume variations (Fig. 4c). In particular, if the monomer enrichment of phase I is less pronounced than the monomer depletion of phase II, the volume of the dense phase V^{I} increases, and vice versa.

An important finding of our work is that the distribution of assembly size evolves differently in each phase (Fig. 4a,b; see SI Movie 1). In phase II, which is initially poor in monomers, assemblies grow slowly toward an equilibrium distribution which monotonously decreases with assembly size following an exponential decay. The kinetics in the initially monomer-rich phase

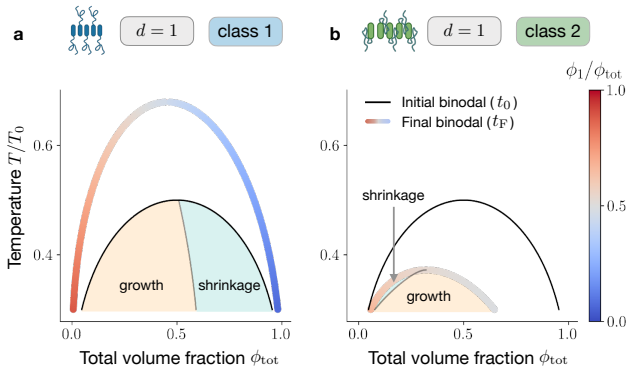

FIG. 5. **Identification of shrinkage and growth regions for different classes**. Here, we study phase-separating systems initially composed of monomers only and we monitor phase volume changes as they relax to thermodynamic equilibrium. **a** For linear assemblies (d=1) belonging to class 1 the final binodal line (coloured curve) is wider than the initial one (black curve), corresponding to monomers and solvent only (black curve). Areas in orange and light blue correspond to growth and shrinkage of the ϕ_{tot}-dense phase (phase I), respectively. **b** The hehaviour of linear assemblies (d=1) belonging belonging to class 2 is remarkably different. Since, in this class, the interaction with the solvent is screened, the final binodal is shrunk compared to the initial one. As a consequence of the shrinkage, the domain corresponding to phase I growth (light blue area) precedes in ϕ_{tot} the shrinkage domain (orange area), for class 2.

I is fundamentally different. First, a very pronounced peak of intermediate-sized assemblies develops quickly. The faster kinetics compared to phase II is caused by monomer diffusion from II to I, which leads to negative feedback for assembly in II and positive feedback in I. This observation is reminiscent of studies on dilute, irreversible aggregation in coexisting phases [39]. The most abundant populations of intermediate-sized assemblies shrink slowly in time feeding the growth of larger assemblies. The resulting equilibrium distribution shows a notable peak of intermediate-sized assemblies followed by an exponential decay. Thus, the difference in the kinetics between the phases is dominantly a consequence of the fact that each phase strives towards a significantly different equilibrium distribution.

IX. ASSEMBLY FORMATION CAN INCREASE OR DECREASE CONDENSATE VOLUME

Here, we discuss changes in phase volumes caused by the assembly kinetics introduced in Sec. VII. In particular, we focus on mixtures initially demixed in two phases, both composed of monomers only, and let the system relax to thermodynamic equilibrium. We then assess for which values of the control parameters ϕ_{tot} and T, the formation of assemblies in both phases leads to a growth of the ϕ_{tot}-rich phase (phase I) and vice versa. More-

over, we distinguish the two protein classes introduced in Sec. IV.

To this end, we compare the phase diagram corresponding to the initial system, composed of monomers only, with the equilibrium phase diagram in which large assemblies populate the mixture. In figure Fig. 5a, we show the initial and final equilibrium binodals (black and coloured curve, respectively), for the case of linear assemblies ($d = 1$) belonging to class 1. In this case, the domain corresponding to demixing enlarges once the system reaches its equilibrium state, i.e., assembly facilitates phase separation. We focus on the $\phi_{\rm tot}$-T domain enclosed by the black curve, where the system is phase separated at all times, and compute the initial and final dense phase volumes via the total volume fraction conservation $V^I(t)/V = (\phi_{\rm tot} - \phi^{\rm II}_{\rm tot}(t))/(\phi^{\rm I}_{\rm tot}(t) - \phi^{\rm II}_{\rm tot}(t))$. As displayed in Fig. 5a, this allows us to identify two parameter regimes: at low $\phi_{\rm tot}$ (orange area), the dense phase grows as assemblies form, while above the dashed grey line (light blue area), it shrinks. Remarkably, linear assemblies ($d = 1$) belonging to class 2 exhibit a completely different behaviour, see Fig. 5b. In this case, assembly formation shrinks the domain corresponding to demixing, thereby suppressing phase separation. In the domain enclosing the coloured curve, we can compute the initial and final dense phase volume for each value of $\phi_{\rm tot}$ and T. In contrast to the previous case, we find that at low $\phi_{\rm tot}$ (light blue area), the dense phase shrinks as assemblies are formed, while for higher $\phi_{\rm tot}$ values (orange area) condensate volume grows, as illustrated in Fig. 5b.

X. CONCLUSION

We extended the classical theory of molecular assembly [14–16] to non-dilute conditions and thereby to regimes where assemblies can phase-separate from the solvent. Our theory relies on a thermodynamic free energy governing the interactions among the constituents. This free energy contains energetic parameters with an assembly size dependence that we obtained by scaling considerations. Our theory applies to reversible and irreversible assembly processes. We showed that the assembly kinetics in each phase is governed by a set of coupled ordinary differential equations if the exchange between the phases is fast compared to the transition rates among assemblies of different sizes. In this limit, we determined the kinetics of size distributions of assemblies in each phase, relaxing toward thermodynamic equilibrium.

Using our theory, we obtained several key findings related to non-dilute conditions and the ability of the assemblies to form a condensed phase. First, size distributions, in general, differ between the phases. In particular, monomers are not necessarily the most abundant species, and distribution tails can significantly deviate from the exponential decay known for classical assembly at dilute conditions. Interestingly, this statement also applies to conditions below the saturation concentration beyond which phase separation can occur. Second, we showed that by lowering the temperature, the dense phase can gelate, i.e., it consists of a single connected assembly of volume equal to the dense phase (a gel). Third, as assemblies form, the volume of the protein-dense phase can grow or shrink depending on the molecular interactions among the constituents.

Our key findings are consistent with recent experimental observations in living cells and in vitro assays using purified proteins. A decrease in droplet volume has been observed in phase-separated condensates composed of purified FUS proteins [55]. Up to now, it has remained unclear whether this kinetics relies on a glass transition as suggested in the discussion of Ref. [55] or on the formation of FUS oligomers in the dense phase. However, a potential hint comes from independent studies, which indicate that FUS can form amyloid-like assemblies, that are associated with neurodegenerative disorders [6], at similar conditions [61, 62]. The transition to a gelated condensate is believed to provide a protection mechanism for the protein expression machinery in the case of intracellular stress. Recent in vitro experiments using purified proteins indicate anomalous size distributions of phase-separating proteins below saturation [24]. More careful experimental measurements using single molecule techniques such as FRET are necessary to scrutinize such preliminary distributions to our theoretical predictions.

Though many biologically-relevant assembly processes are reversible and governed by thermodynamic principles, there are also a large number of assemblies that are persistently maintained away from equilibrium. An important class is assemblies where the formation or disassembly relies on the hydrolysis of a fuel component such as ATP or GTP turning over to the corresponding waste, ADP or GDP. Since the fuel levels are kept constant in living cells, fuel-driven assembly processes are maintained away from equilibrium and thus cannot relax to thermodynamic equilibrium. It is an exciting extension of our work to consider fuel and waste components and how distributions of assembly sizes and the gelation of condensates are affected when maintained away from equilibrium.

Appendix A: Scaling laws for internal and interaction energies

Here we provide a physical interpretation of the internal free energy ω_i. For simplicity, we consider a homogeneous system solely composed of assemblies of size i, characterized by the volume fraction vector $\phi^{(i)}$, with $\phi^{(i)}_i = 1$ and $\phi^{(i)}_j = 0$ for $i \neq j$. Making use of Eq. (1), the internal free energy of such systems can be written as

$$\omega_i = f(\phi^{(i)})\nu_1 - k_B T\, i^{-1} \ln i^{-1}\,, \tag{A1}$$

with $f(\phi^{(i)})\nu_1$ being the free energy associated with each monomer belonging to the i-th assembly. The second

term in the equation above is the conformational entropy that stems from having more accessible states with increasing assembly size. Thus, Eq. (A1) allows interpreting ω_i as the free energy of monomers inside an assembly of size i, coming only from bonds between monomers. To quantify it, we introduce the number of binding sites for each monomer, z. Following Ref. [16], we distinguish between n_b monomers at the boundaries of the assembly, and $(i-n_\mathrm{b})$ in the assembly bulk. Monomers in the bulk can saturate all their z binding sites while, in general, monomers at the boundaries are able to saturate only $z_\mathrm{b} < z$. Thus, we get

$$\begin{aligned}\omega_i &= \frac{z(i-n_\mathrm{b}) + z_\mathrm{b} n_\mathrm{b}}{2i}\,\Delta\omega \\ &= \frac{z}{2}\,\Delta\omega - (z-z_\mathrm{b})\frac{n_\mathrm{b}}{2i}\,\Delta\omega\,,\end{aligned} \tag{A2}$$

where $\Delta\omega = e_\mathrm{int} - T s_\mathrm{int}$ is the free energy associated with the formation of every single bond, decomposed in its energetic and entropic contribution, e_int and s_int, respectively. The factor two avoids double counting.

We describe three species of assemblies: rod-like, disc-like and spherical. These can be realised by varying the number of binding sites and their orientation. Rod-like assemblies ($d = 1$) are defined to have only two binding sites with a fixed orientation. They can be pictured as one-dimensional assemblies with no loops, leading to $n_\mathrm{b} = 2$, $z = 2$ and $z_\mathrm{b} = 1$. Disk-like assemblies ($d = 2$) are defined to have $z > 2$ co-planar binding sites, for which $n_\mathrm{b} \simeq \sqrt{i}$. Spherical assemblies ($d = 3$) are characterized by $z > 2$ binding sites with no precise orientation leading to $n_\mathrm{b} \simeq i^{\frac{2}{3}}$. Summing up, we get

$$n_\mathrm{b} \simeq i^{\frac{d-1}{d}}\,, \tag{A3}$$

that inserted in Eq. (A2) leads to Eq. (8), recalling that $\Delta\omega = e_\mathrm{int} - T s_\mathrm{int}$.

In this equation, we grouped the constant terms in ω_∞, which does not affect chemical equilibrium, since they drop in any chemical potential difference that drives chemical transitions. Moreover, ω_∞ does also not affect phase equilibrium. However, in the case of $d = 2, 3$ and $M \to \infty$, ω_∞ is important to study the gelation of the dense phase, see App. C. In Eq. (8), the second term represents a boundary interaction penalty, accounting for the fact that monomers at the assembly boundary can realise fewer internal bonds than monomers at the assembly bulk, in analogy with the physical origin of surface tension.

We now discuss the size dependence of the interaction parameters χ_{ij}. Starting from a lattice model, these parameters can be expressed in terms of the energetic parameters e_{ij} corresponding to having two neighbouring monomers belonging to i and j. In particular, $\chi_{ij} = 2e_{ij} - e_{ii} - e_{jj}$. Assuming that the energies associated with monomer-monomer interactions do not vary within assemblies, i.e., $e_{ij} = e_{11}$ is constant, we get $\chi_{ij} = 0$. Moreover, we now discuss the scaling of

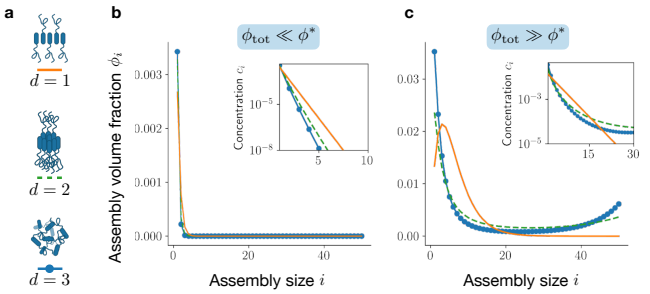

FIG. 6. **A volume fraction threshold separates two assembly regimes in homogeneous systems**. **a** Illustration of assemblies belonging to Class 1 with different spatial dimension. **b** Assembly size distribution for $M = 50$, at low total macromolecular volume fraction: $\phi_\mathrm{tot} \ll \phi^*$. Disregarding assembly dimension, d, the macromolecules are mainly in the monomer state, i.e., $\phi_1 \simeq \phi_\mathrm{tot}$. **c** For $\phi_\mathrm{tot} \gg \phi^*$, the monomer concentration saturates at $\phi_1 \simeq \phi^*$ and big assemblys begin to populate the system. For rod-like assemblies (corresponding to $d = 1$ in Eq. (8)), the distribution becomes peaked at an intermediate value $i_\mathrm{max} > 1$ and then exponentially cut off. For disk-like and spherical assemblies, $d = 2, 3$, the distribution becomes bimodal, with peaks at $i = 1$ and $i = M$, the maximum assembly size ($M = 50$). This bimodal behaviour hints at the emergence of a gelation transition in the limit $M \to \infty$. In the insets, we show the scaling of concentrations c_i with assembly size. For $d = 2, 3$ and above the ϕ^* threshold, we find deviations from the classical exponential decay.

$\chi_{is} = 2e_{is} - e_{ii} - e_{ss}$. If the monomer-solvent interactions are also chosen to be size-independent, i.e., $e_{is} = e_{1s}$, we get $\chi_{is} = 2e_{1s} - e_{11} - e_{ss} = \chi$. This explains the scaling in Class 1 (see Eq. (9)).

However, many proteins of interest screen their hydrophobic interaction when forming assemblies [2, 45, 54] implying that the interactions between monomers in assembly i with solvent (s) e_{is} varies with assembly size i. In each assembly, this energy per monomer comes from two contributions. The first corresponds to monomers in the bulk which are $(n - n_\mathrm{b})$ and have interaction with solvent e'_{1s}. The second one corresponds to the n_b monomers at the assembly boundary, characterised by interaction with solvent e_{1s}. We get

$$e_{is} = \frac{e'_{1s}(i-n_\mathrm{b}) + e_{1s} n_\mathrm{b}}{i}\,. \tag{A4}$$

Using the scaling of n_b/i already introduced above in the discussion of the internal free energy scaling, see A3, we obtain Eq. (10).

by abbreviating $\chi'_{is} = 2e'_{1s} - e_{11} - e_{ss} =: \chi$; this case corresponds to Class 2.

Appendix B: Linear assemblies belonging to class 1

For class 1 and $d = 1$, Eq. (4) reads

$$\phi_i = i \left(\frac{\phi_1}{\tilde{\phi}}\right)^i \tilde{\phi}\,, \tag{B1}$$

where we have introduced the characteristic volume fraction

$$\tilde{\phi} = \exp\left(\frac{e_{\rm int} - s_{\rm int} T}{k_B T} - 1\right). \tag{B2}$$

It is straightforward to verify that the latter volume fraction is proportional to the assembly threshold defined in Eq. (11), i.e. $\tilde{\phi} = \mathrm{e}/(1-\mathrm{e})^2\phi^*$. In Fig. 6, we show the assembly size distribution in homogeneous mixtures obtained by numerically solving Eq. (4) together with Eq. (5), with a cut-off $M = 50$. We characterise the behaviour of assemblies with different spatial dimensions $d = 1, 2, 3$, see Fig. 6a. For dilute solutions, corresponding to $\phi_{\rm tot} \ll \phi^*$, the size distribution is dominated by monomers while larger assemblies have vanishing volume fraction, i.e., $\phi_1 \simeq \phi_{\rm tot}$, see Fig. 6b. For $\phi_{\rm tot} \gg \phi^*$, the monomer concentration saturates at $\phi_1 \simeq \phi^*$ and assemblies begin to populate the system. As depicted in Fig. 6b, above this threshold the size distribution depends crucially on assembly dimension d. For rod-like assemblies ($d = 1$ in Eq. (8)), the distribution becomes peaked at a value $M > 1$ and then exponentially decays. For disk-like and spherical assemblies, $d = 2, 3$ in Eq. (8), the distribution becomes bimodal peaked at $i = 1$ and $i = M$, the maximum assembly size ($M = 50$ in Fig. 6c). The behaviour of the system at high density can be quantitatively studied by performing the thermodynamic limit, i.e., $M \to \infty$. Within this limit, the series defined in the conservation law, Eq. (5) can be explicitly solved, leading to

$$\frac{\phi_1}{\tilde{\phi}} = \frac{1 + 2\frac{\phi_{\rm tot}}{\tilde{\phi}} - \sqrt{1 + 4\frac{\phi_{\rm tot}}{\tilde{\phi}}}}{2\frac{\phi_{\rm tot}}{\tilde{\phi}}}\,. \tag{B3}$$

Recalling that $\tilde{\phi} = \mathrm{e}/(1-\mathrm{e})^2\phi^*$, this leads to $\phi_1 \simeq \phi_{\rm tot}$, in the regime $\phi_{\rm tot} \ll \phi^*$, while for $\phi_{\rm tot} \gg \phi^*$, we get $\phi_1 \simeq \phi^*$.

The maximum of the volume fraction distribution in Eq. (B1) can be obtained imposing $\partial_i \phi_i = 0$, leading to

$$i_{\rm max} = \frac{1}{\ln\left(\tilde{\phi}/\phi_1\right)} \simeq \sqrt{\frac{\phi_{\rm tot}}{\tilde{\phi}}}\,. \tag{B4}$$

The approximate expression on the right hand is obtained using Eq. (B3) and expanding for $\phi_{\rm tot}/\tilde{\phi} \gg 1$.

The average $\langle i \rangle = \sum i\phi_i / \sum \phi_i$ is given by

$$\langle i \rangle = \frac{\phi_1}{\phi_{\rm tot}} \frac{3 - \phi_1/\tilde{\phi}}{(1 - \phi_1/\tilde{\phi})^3} \simeq 2\, i_{\rm max}\,, \tag{B5}$$

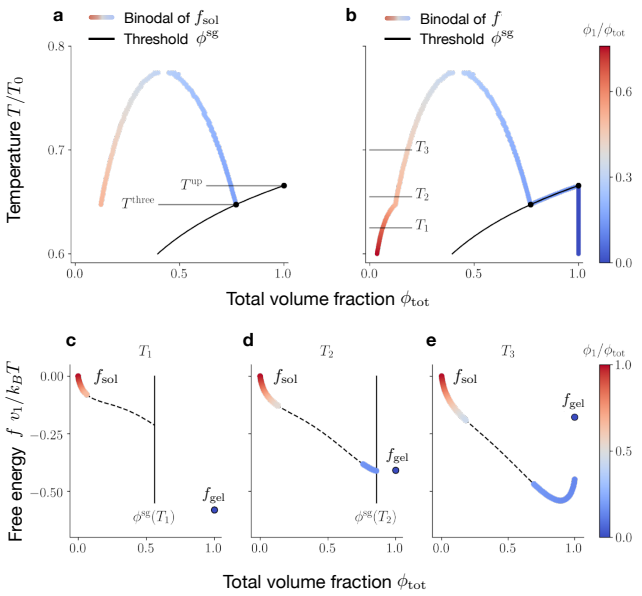

FIG. 7. **Gel-sol free energies**. **a** The coloured curved indicates the binodal obtained with the Maxwell construction for the $f_{\rm sol}$ only, its colour code depicting the monomer fraction $\phi_1/\phi_{\rm tot}$ in the coexisting phases. The black line represents $\phi^{\rm sg}(T)$, defined in Eq. (C2). In the absence of phase separation, $\phi^{\rm sg}$ estimates the volume fraction at which the gel appears. The two temperatures $T^{\rm three}$ and $T^{\rm up}$ are used to determine the value of ω_∞ in $f_{\rm gel}$, see Eq. (13). This allows us to perform the Maxwell construction now on $f = f_{\rm sol} + f_{\rm gel}$. **b** In phase-separating systems, gelation can be considered as a special case of phase coexistence between a dilute phase (the "sol") in which $\phi^{\rm sol} < 1$ and the gel phase, corresponding to $\phi^{\rm gel} = 1$. **c-e** Maxwell construction for three different temperature values, the coloured and dashed curves represent convex and concave branches of f, respectively.

where we expanded for $\phi_{\rm tot}/\tilde{\phi} \gg 1$ to obtain the approximate expression.

We can also derive an expression for the free energy as a function of the conserved quantity alone $\phi_{\rm tot}$, making use of Eq. (B1) together with Eq. (B3):

$$f_{\rm sol} = \frac{k_B T}{\nu_1}\left[(1-\phi_{\rm tot})\ln(1-\phi_{\rm tot}) + \phi_{\rm tot}\ln\frac{\phi_1}{\tilde{\phi}} - \frac{\phi_1}{1-\phi_1/\tilde{\phi}} + \frac{\chi}{k_B T}\phi_{\rm tot}(1-\phi_{\rm tot})\right]. \tag{B6}$$

Appendix C: Gelation transition for two and three-dimensional assemblies

As outlined in Fig. 6 for $d = 2, 3$, at high $\phi_{\rm tot}$ for M finite, the size distribution shows a bimodal behaviour. This suggests for the limit $M \to \infty$ that the system undergoes a gelation transition, which is defined as the emergence of an assembly that is comparable with the

system size [16, 37, 38]. To precisely locate the $\phi_{\rm tot}$ value at which the transition occurs, we recall Eq. (4) and consider the series

$$\sum_{i=1}^{\infty}\phi_i=\sum_{i=1}^{\infty} i\left(\frac{\phi_1}{\tilde{\phi}}\right)^i \exp\left(\frac{\Delta\omega}{k_BT}\,i^{\frac{d-1}{d}}-1\right). \qquad \text{(C1)}$$

We note that when $N\to\infty$, this series converges only if $\phi_1/\tilde{\phi}\le 1$. Thus, we get an upper bound for the series, namely

$$\sum_{i=1}^{\infty}\phi_i\le\sum_{i=1}^{\infty} i\,\exp\left(\frac{\Delta\omega}{k_BT}\,i^{\frac{d-1}{d}}-1\right)\equiv\phi^{\rm sg}. \qquad \text{(C2)}$$

Approximating the series with the integral, we get an estimation for $\phi^{\rm sg}$:

$$\phi^{\rm sg}=\begin{cases}2\frac{\left(6-6\Delta\omega+3\Delta\omega^2-\Delta\omega^3\right)}{\Delta\omega^4}\tilde{\phi}\,, & d=2\,,\\ -\frac{3}{2}\frac{\Delta\omega^3}{(2-2\Delta\omega+\Delta\omega^2)}\tilde{\phi}\,, & d=3\,.\end{cases} \qquad \text{(C3)}$$

By a Maxwell construction, Eq. (7) with free energy Eq. (12), we can study the interplay between the gelation transition and phase separation. To ensure that at high $\phi_{\rm tot}$, where we expect no phase separation to occur, the system gelates at $\phi_{\rm tot}=\phi^{\rm sg}$ we chose

$$\omega_\infty=e_\infty-Ts_\infty\,. \qquad \text{(C4)}$$

In particular, we need two conditions to fix e_∞ and s_∞. For this purpose, we first perform the Maxwell construction on the $f_{\rm sol}$ contribution only. In Fig. 7a, we display the result of the construction, coloured curve, together with the gelation threshold $\phi^{\rm sg}(T)$, black line. Here, the coloured curve represents the binodal, and its colour code depicts the monomer fraction $\phi_1/\phi_{\rm tot}$ in the coexisting phases. In the regime where both binodal branches lie below the gelation threshold, we indeed expect $f_{\rm sol}$ to be the only relevant contribution to f. This allows us to locate the temperature $T^{\rm three}$ at which the binodal and $\phi^{\rm sg}$ intersect. Imposing at $T^{\rm three}$ that the $f_{\rm gel}$ is such that the system exhibits three-phase coexistence between the two binodal points and the gel, gives the first condition to determine ω_∞. For the second condition, we start locating upper gelation temperature $T^{\rm up}$, at which $\phi^{\rm sg}(T)=1$. Then we impose the volume fractions of the two coexisting phases collapse to 1 at the upper gelation temperature, i.e $\phi_{\rm tot}^{\rm I/II}\to 1$ for $T\to T^{\rm up}$. These two conditions uniquely determine e_∞ and s_∞ and thus ω_∞ through Eq. (C4). We can now use the full $f=f_{\rm sol}+f_{\rm gel}$ in the Maxwell construction. The result of the construction is displayed in Fig. 7b. Notice that the binodal and the gelation threshold $\phi^{\rm sg}(T)$ are indeed overlapping. In Fig. 7, we display the free energy for three temperature values corresponding to sol-gel coexistence (Fig. 7c), sol-sol and sol-gel coexistence (Fig. 7d), and sol-sol coexistence only (Fig. 7e). The dashed lines represent values where f is not convex. Notice that, for consistency, we use values of $f_{\rm sol}$ only up to $\phi^{\rm sg}$ (denoted by a vertical black line).

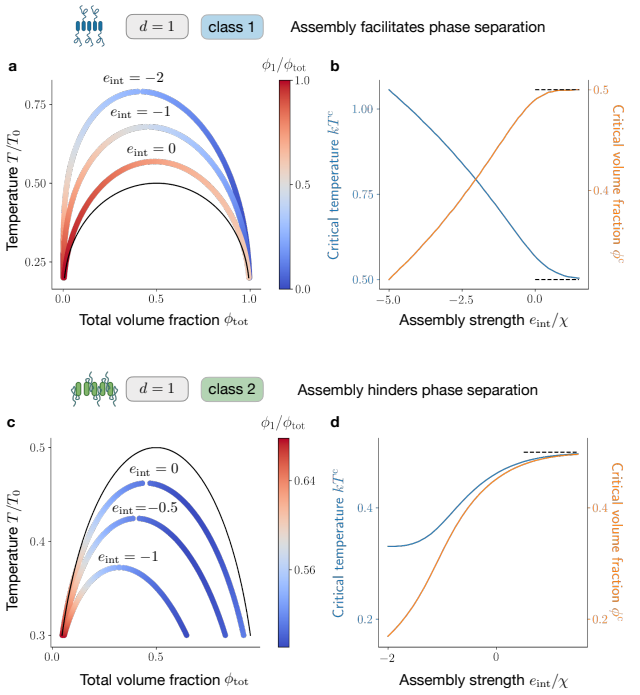

FIG. 8. **The influence of assemblies on the system phase behaviour**. **a** Focusing on systems with $d=1$ belonging to class 1, we compare three binodals corresponding to assembly strength $e_{\rm int}/\chi=0.5,-1,-2$ (coloured curves) and the reference binary mixture composed of monomers and solvent only (black curve). The latter can be associated with the limit $e_{\rm int}/\chi\to\infty$. The region enclosed by the binodal, corresponding to phase separation, expands even for assemblies with no assembly energy $e_{\rm int}/\chi=0$. This can be explained by the entropic advantage caused by size polydispersity. **b** Dependence of the critical volume fraction and critical temperature on the assembly strength $e_{\rm int}/\chi$. The presence of assemblies causes T^c and ϕ^c to deviate from the reference values (black dashed lines) corresponding to a binary mixture with monomers and solvent only ($e_{\rm int}/\chi\to\infty$). In particular, for Class 1, making assemblies more energetically favourable, i.e. decreasing $e_{\rm int}/\chi$, induces an increase in T^c and a decrease in ϕ^c, in turn making phase separation more accessible. **c** Comparison between three binodal lines corresponding to systems belonging to class 2 and $d=1$, with assembly energies $e_{\rm int}/\chi=0,-0.5,-1$ (coloured curves) and the reference binary mixture composed of monomers and solvent only (black curve). **d** For Class 2, decreasing $e_{\rm int}/\chi$, causes T^c and ϕ^c to decrease, overall hindering phase separation. This is caused by the interaction propensity screening in monomers at the bulk of assemblies belonging to class 2, see Eq. (10)

Appendix D: Mutual feedback between phase separation and assembly equilibria

We first discuss how assemblies can shape the phase diagram. For linear assemblies ($d=1$) belonging to Class 1, assemblies facilitate phase separation. Indeed, as illustrated in Fig. 8a-b, increasing the relative assembly strength, i.e., decreasing $e_{\rm int}/\chi$, leads to an upshift

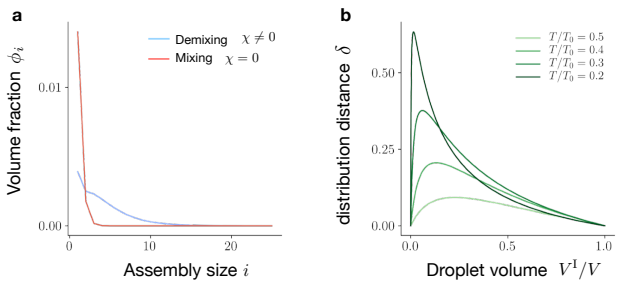

FIG. 9. **The influence of phase separation on assembly size**. **a** Comparison between the size distribution in a homogeneous system, and in the corresponding phase-separated system (averaged in both compartments). Here, we consider rod-like assemblies ($d = 1$), $M \to \infty$, $\phi_{\mathrm{tot}} = 0.016$ and $T/T_0 = 0.2$. We note that the presence of compartments can favour assembly formation, even when the corresponding homogeneous mixture is populated mainly by monomers. The difference in distributions can be quantified utilizing the functional distance, defined in Eq. (D2). **b** The magnitude of this distance depends on the droplet size and the temperature chosen. The volume corresponding to the maximum distribution distance shifts towards lower values with decreasing temperature $T/T0$. The distributions separated by the maximum distance, for $T/T0 = 0.2$, are the ones displayed in **a**

in critical temperature and a downshift in critical volume fraction. This trend can be explained by considering that assembly formation, even if energetically disfavoured, reduces the mixing entropy (see the first term in Eq. (1)). In Fig. 8a, we show the binodal lines corresponding to three representative values of the assembly strength: $e_{\mathrm{int}}/\chi = 0, -1, -2$. We compare them to the black curve, which corresponds to a binary mixture made of monomers and solvent only (black curve). This reference case can be thought of as the limiting case in which assemblies have an infinite energy penalty, i.e, $e_{\mathrm{int}}/\chi =\to \infty$. In Fig. 8b, we quantify the changes in critical temperature and critical volume fraction as a function of the relative assembly strength e_{int}/χ. In Fig. 8c-d, we illustrate the behaviour of linear assemblies ($d = 1$) belonging to Class 2. In contrast to Class 2, assemblies can suppress phase separation. Indeed, making assemblies more favourable by decreasing e_{int}/χ, the critical temperature decreases, and even if the critical density decreases and the binodal shrinks, see Fig. 8c. In Fig. 8d, we display critical temperatures and critical volume fraction variations as a function of the relative assembly strength e_{int}/χ.

Fig. 8 clearly shows that the presence of assemblies affects the phase equilibrium of a mixture. We now prove that, in turn, the total number of assemblies can differ between phase-separating and homogeneous systems with the same total protein volume fraction. To show this, we fix the interaction propensity χ, the temperature T/T_0, and the total macromolecule volume fraction ϕ_{tot} to values corresponding to two-phase coexistence at thermodynamic equilibrium. We then compare the assembly size distribution (after averaging over both phases), with the distribution in the corresponding homogeneous state, with the same values of T and ϕ_{tot}. Recalling that due to our choice of interaction propensity scaling in Eq. (9) that the size distribution in the homogeneous system, Eq. (4), does not depend on χ. For this reason, the homogeneous state can be thought of as an unstable state corresponding to the same χ as the phase separating one, which has not reached phase equilibrium yet, but also as the equilibrium state of a system with the same parameters as the phase separating one, but formed by assemblies that do not interact with the solvent ($\chi = 0$).

In Fig. 9a, we display results for rod-like assemblies ($d = 1$) with $T/T_0 = 0.2$, and $\phi_{\mathrm{tot}} = 0.016$. We compare the size distribution in the homogeneous system ϕ_i^{h}, with the weighted average over compartments, defined as

$$\bar{\phi}_i = \frac{V^{\mathrm{I}}}{V}\phi_i^{\mathrm{I}} + \frac{V^{\mathrm{II}}}{V}\phi_i^{\mathrm{II}}\,, \tag{D1}$$

in the corresponding phase-separated system. Clearly, the two distributions differ, showing that the presence of compartments can lead to larger assemblies. The difference in size distributions can be quantified utilizing the so-called total variation distance, defined as

$$\delta(h, g) = \sup_i \left| \frac{h_i}{\sum_i h_i} - \frac{g_i}{\sum_i g_i} \right| . \tag{D2}$$

This quantity characterizes the distance between two normalised functions as the largest possible distance among values that they assign to the same argument. The distance between the homogeneous size distribution and the distribution defined in Eq. (D1) depends on the temperature T and the total volume fraction ϕ_{tot}, which in turn determines the droplet size. In Fig. 9b, we display distribution distances $\delta(\phi^{\mathrm{h}}, \bar{\phi})$ corresponding to different temperatures and droplet volumes. In the limits $V^{\mathrm{I}}/V \to 0$ and $V^{\mathrm{I}}/V \to 1$, the system becomes homogeneous. As a result, the distribution distance $\delta(\phi^{\mathrm{h}}, \bar{\phi})$ vanishes. Note that the volume corresponding to the maximum distribution distance shifts towards lower values.

Appendix E: Assembly kinetics in homogeneous mixtures

In this section, we give the details on the kinetic theory for assembly in non-dilute homogeneous systems that can relax toward chemical equilibrium. Each component i follows

$$\frac{\mathrm{d}\phi_i}{\mathrm{d}t} = r_i\,. \tag{E1}$$

Focusing on monomer exchange among assemblies, the assembly rates read

$$\begin{aligned} r_1 &= -\Delta r_1 - \sum_{i=1}^{M-1} i\Delta r_i\,, \\ r_i &= (i-1)\Delta r_{i-1} - i\,\Delta r_i\,, \qquad \text{for } i = 2,..M-1\,, \\ r_M &= (M-1)\,\Delta r_{M-1}\,. \end{aligned} \tag{E2}$$

These rates conserve the total volume fraction $\phi_{\rm tot}$, i.e., $\partial_t\phi_{\rm tot} = \partial_t \sum_i r_i\, i = 0$. The assembly flux $(i = 2, ...M)$

$$\Delta r_i = s_i \left[1 - \exp\left(\frac{(i+1)\mu_{i+1} - i\mu_i - \mu_1}{k_B T}\right)\right]\,. \tag{E3}$$

is determined by differences in chemical potential per monomer.

For assemblies of class 1, we can use the chemical potential Eq. (2) and write the assembly flux as

$$\Delta r_i = s_i \left(1 - \frac{i}{i+1}\frac{\phi_{i+1}}{\phi_i\,\phi_1} K_i^{-1}\right)\,, \tag{E4}$$

where we have introduced

$$K_i = \exp\left(1 - \frac{(i+1)\omega_{i+1} - i\omega_i - \omega_1}{k_B T}\right)\,. \tag{E5}$$

We chose $s_i = \phi_i\phi_1 K_i/\phi_i\, s$ in order to recover a finite rate in the limit $\phi_1, \phi_i \ll 1$. We finally recast the flux in Eq. (E2) as

$$\Delta r_i = s\left(\frac{\phi_i\phi_1}{i}\,K_i - \frac{\phi_{i+1}}{i+1}\right)\,. \tag{E6}$$

Eq. (E5) is the assembly kernel. In general, this kernel depends on the assembly size i. However, for rod-like assemblies $(d = 1)$, the assembly kernel $K_i = K = \exp\left(1 + \frac{\Delta\omega}{k_B T}\right)$ is independent of size i [15].

Appendix F: Assembly kinetics in compartments

Here, we generalise the assembly kinetics described in the previous section to the case of phase coexistence. To this end, we focus on passive systems that can relax toward thermodynamic equilibrium. Moreover, we restrict ourselves to systems that are at phase equilibrium at any time during the relaxation kinetics toward thermodynamic equilibrium and following the theory originally developed in Ref. [56]. Chemical kinetics constrained to phase equilibrium is valid if the chemical reaction rates are small compared to diffusion rates. By choosing initial average volume fractions corresponding to two-phase coexistence, we can consider the system volume to be divided into two homogeneous compartments as a result of phase separation. We then study the time evolution of

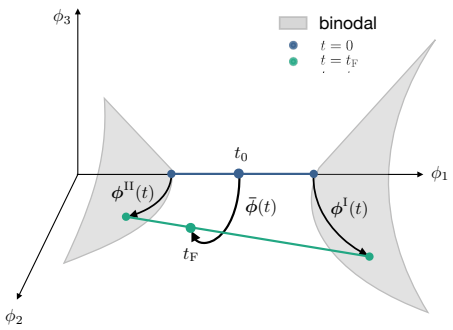

FIG. 10. **Kinetic trajectory in the multicomponent phase diagram** Illustration of the assembly kinetics at phase equilibrium, for systems corresponding to $M = 3$ and initially composed of monomers only.

compartment sizes and volume fractions due to chemical reactions, enforcing instantaneous phase equilibrium at all times. To this aim, we start with the variation of particle numbers in compartments I and II:

$$\frac{{\rm d}N_i}{{\rm d}t}^{\rm I/II} = -J_i^{\rm I/II} + R_i^{\rm I/II}\,, \tag{F1}$$

where $R_i^{\rm I/II}$ are the variations due to chemical reactions and $J_i^{\rm I/II}$ describes the exchange of assemblies between the two phases. Particle conservation during crossing implies $J_i^{\rm I} = -J_i^{\rm II}$. Due to volume conservation in the two-phase, we have

$$V^{\rm I/II} = \sum_{i=0}^{M} N_i^{\rm I/II} v_i\,. \tag{F2}$$

Furthermore, $V = V^{\rm I} + V^{\rm II}$. We now introduce volume fractions $\phi_i^{\rm I/II} = N_i^{\rm I/II}/V^{\rm I/II}$ and the rescaled rates $j_i^{\rm I/II} = v_i\, J_i^{\rm i/II}/V^{\rm I/II}$ and $r_i^{\rm I/II} = v_i\, R_i^{\rm I/II}/V^{\rm I/II}$, leading to

$$\frac{{\rm d}\phi_i}{{\rm d}t}^{\rm I/II} = -j_i^{\rm I/II} + r_i^{\rm I/II} - \phi_i^{\rm I/II}\,\frac{{\rm d}\ln V}{{\rm d}t}^{\rm I/II}\,, \tag{F3}$$

which correspond to Eq. (E1) generalised two-phase coexistence. We can write the rates in both phases as

$$\begin{aligned} r_1^{\rm I/II} &= -\Delta r_1^{\rm I/II} - \sum_{i=1}^{M-1} i\,\Delta r_i^{\rm I/II}\,, \\ r_i^{\rm I/II} &= (i-1)\Delta r_{i-1}^{\rm I/II} - i\,\Delta r_i^{\rm I/II} \qquad \text{for } i = 2,..M-1\,, \\ r_M^{\rm I/II} &= (M-1)\Delta r_{M-1}^{\rm I/II}\,, \end{aligned} \tag{F4}$$

with

$$\Delta r_i = s\left(\frac{\phi_i^{\rm I/II}\,\phi_1^{\rm I/II}}{i} K_i - \frac{\phi_{i+1}^{\rm I/II}}{i+1}\right)\,, \tag{F5}$$

where the assembly kernel is defined in Eq. (E5). Eq. (F1) and Eq. (F2) can be combined to get $\mathrm{d}_t V^{\mathrm{I/II}} = V^{\mathrm{I/II}} \sum_{i=0}^{M} (r_i^{\mathrm{I/II}} - j_i^{\mathrm{I/II}})$. Using the volume conserving properties of the rates, $\sum_{i=0}^{M} r_i^{\mathrm{I/II}} = 0$, we finally get

$$\frac{\mathrm{d} \ln V^{\mathrm{I/II}}}{\mathrm{d}t} = -\sum_{i=0}^{M} j_i^{\mathrm{I/II}} . \tag{F6}$$

Assembly mass conservation at the interface implies

$$j_i^{\mathrm{I}} = -j_i^{\mathrm{II}} \frac{V^{\mathrm{II}}}{V^{\mathrm{I}}} , \tag{F7}$$

with the volume dynamics obeying $\mathrm{d}_t(V^{\mathrm{I}} + V^{\mathrm{II}}) = 0$.

The currents $j_i^{\mathrm{I/II}}$ satisfy that phase equilibrium is satisfied at all times, which can be expressed by taking a time derivative of Eq. (7):

$$\sum_{j=0}^{M} \frac{\partial \mu_i^{\mathrm{I}}}{\partial \phi_j^{\mathrm{I}}} \frac{\mathrm{d}\phi_j^{\mathrm{I}}}{\mathrm{d}t} = \sum_{j=0}^{M} \frac{\partial \mu_i^{\mathrm{II}}}{\partial \phi_j^{\mathrm{II}}} \frac{\mathrm{d}\phi_j^{\mathrm{II}}}{\mathrm{d}t} , \tag{F8a}$$

$$\sum_{j=0}^{M} \frac{\partial \Pi^{\mathrm{I}}}{\partial \phi_j^{\mathrm{I}}} \frac{\mathrm{d}\phi_j^{\mathrm{I}}}{\mathrm{d}t} = \sum_{j=0}^{M} \frac{\partial \Pi^{\mathrm{II}}}{\partial \phi_j^{\mathrm{II}}} \frac{\mathrm{d}\phi_j^{\mathrm{II}}}{\mathrm{d}t} , \tag{F8b}$$

provided that the initial phase volume and volume fractions $V^{\mathrm{I}}(t=0)$, and $\phi_i^{\mathrm{I/II}}(t=0)$ are a solution of Eq. (7). Once an expression for $\partial\mu_i/\partial\phi_j$ and $\partial\Pi/\partial\phi_j$ is calculated, we can derive an a set of $M+1$ equations for j_i^{I} inserting Eq. (F3), Eq. (F6), and Eq. (F7) in Eq. (F8). These equations are linear and enable us to find an expression for $j_i^{\mathrm{I/II}}$ as a function of $\phi_i^{\mathrm{I/II}}$ and V^{I}/V. We have finally all the ingredients to characterize the dynamics of the phase volume and volume fractions $\phi_i^{\mathrm{I/II}}(t)$ and $V^{\mathrm{I}}(t)$, integrating Eq. (F3) and Eq. (F6) and provided we can solve the initial phase equilibrium problem to find $V^{\mathrm{I}}(t=0)/V$, and $\phi_i^{\mathrm{I/II}}(t=0)$. This scheme can be used to study the kinetics of a system initially composed of two phases filled by monomers only that relax to its thermodynamic equilibrium. An example of such relaxation kinetics is depicted in Fig 10. Note that the currents $j_i^{\mathrm{I/II}}$ restrict the trajectories to lie in the binodal manifold at all times.

ACKNOWLEDGMENTS

We thank J. Bauermann, K. Alameh, I. Haugerud, P. McCall, T. Harmon, L. Hubatsch, L. Jawerth and F. Jülicher for fruitful discussions about the topic. We thank C. Seidel and T. Franzmann for pointing out the relevance of your theory for protein aggregation in biomolecular condensates. We acknowledge J.-F. Joanny for pointing out the references [35, 37]. We thank J. Bauermann, S. Horvát and C. Duclut for help improving the Mathematica code. A very special thanks go to I. Haugerud for very helpful feedback on the manuscript. G. Bartolucci and C. Weber acknowledge the SPP 2191 "Molecular Mechanisms of Functional Phase Separation" of the German Science Foundation for financial support. C. Weber acknowledges the European Research Council (ERC) under the European Union's Horizon 2020 research and innovation programme (Fuelled Life, Grant Number 949021) for financial support. Figures created with BioRender.com.

[1] P. Doty and G. E. Myers, Discussions of the Faraday Society **13**, 51 (1953), ISSN 0366-9033.
[2] M. P. Hughes, M. R. Sawaya, D. R. Boyer, L. Goldschmidt, J. A. Rodriguez, D. Cascio, L. Chong, T. Gonen, and D. S. Eisenberg, Science **359**, 698 (2018), ISSN 0036-8075, 1095-9203.
[3] A. W. Fritsch, A. F. Diaz-Delgadillo, O. Adame-Arana, C. Hoege, M. Mittasch, M. Kreysing, M. Leaver, A. A. Hyman, F. Jülicher, and C. A. Weber, Proceedings of the National Academy of Sciences **118**, e2102772118 (2021).
[4] S. F. Banani, H. O. Lee, A. A. Hyman, and M. K. Rosen, Nature Reviews Molecular Cell Biology **18**, 285 (2017), ISSN 1471-0080.
[5] E. Nüske, G. Marini, D. Richter, W. Leng, A. Bogdanova, T. M. Franzmann, G. Pigino, and S. Alberti, Biology Open **9**, bio046391 (2020), ISSN 2046-6390.
[6] A. Zbinden, M. Pérez-Berlanga, P. De Rossi, and M. Polymenidou, Developmental Cell **55**, 45 (2020), ISSN 15345807.
[7] B. Wang, L. Zhang, T. Dai, Z. Qin, H. Lu, L. Zhang, and F. Zhou, Signal Transduction and Targeted Therapy **6**, 290 (2021), ISSN 2059-3635.
[8] S. Alberti, A. Gladfelter, and T. Mittag, Cell **176**, 419 (2019), ISSN 0092-8674.
[9] Y. G. Zhao and H. Zhang, Developmental Cell **55**, 30 (2020), ISSN 15345807.
[10] J. Agudo-Canalejo, S. W. Schultz, H. Chino, S. M. Migliano, C. Saito, I. Koyama-Honda, H. Stenmark, A. Brech, A. I. May, N. Mizushima, et al., Nature **591**, 142 (2021), ISSN 0028-0836, 1476-4687.
[11] L. Babl, A. Merino-Salomón, N. Kanwa, and P. Schwille, Scientific Reports **12**, 17949 (2022), ISSN 2045-2322.
[12] T. Lu, S. Liese, L. Schoenmakers, C. A. Weber, H. Suzuki, W. T. S. Huck, and E. Spruijt, Journal of the American Chemical Society **144**, 13451 (2022), ISSN 0002-7863.
[13] C. A. Weber, D. Zwicker, F. Jülicher, and C. F. Lee, Reports on Progress in Physics **82**, 064601 (2019), ISSN 0034-4885, 1361-6633.
[14] W. H. Stockmayer, The Journal of Chemical Physics **11**, 45 (1943), ISSN 0021-9606, 1089-7690.
[15] P. L. Krapivsky, S. Redner, and E. Ben-Naim, *A Kinetic*

View of Statistical Physics (Cambridge University Press, Cambridge, 2010), ISBN 978-0-521-85103-9.

[16] J. N. Israelachvili, *Intermolecular and Surface Forces* (Academic Press, 2015), ISBN 978-0-08-092363-5.

[17] A. C. Dumetz, A. M. Chockla, E. W. Kaler, and A. M. Lenhoff, Biophysical Journal **94**, 570 (2008), ISSN 00063495.

[18] Y. Shin and C. P. Brangwynne, Science **357**, eaaf4382 (2017), ISSN 0036-8075, 1095-9203.

[19] P. M. McCall, S. Srivastava, S. L. Perry, D. R. Kovar, M. L. Gardel, and M. V. Tirrell, Biophysical Journal **114**, 1636 (2018), ISSN 0006-3495.

[20] T. Wiegand and A. A. Hyman, Emerging Topics in Life Sciences **4**, 247 (2020), ISSN 2397-8554, 2397-8562.

[21] Z. Liu, Y. Yang, A. Gu, J. Xu, Y. Mao, H. Lu, W. Hu, Q.-Y. Lei, Z. Li, M. Zhang, et al., Nature Communications **11**, 2266 (2020), ISSN 2041-1723.

[22] A. M. Küffner, M. Linsenmeier, F. Grigolato, M. Prodan, R. Zuccarini, U. C. Palmiero, L. Faltova, and P. Arosio, Chemical Science **12**, 4373 (2021), ISSN 2041-6539.

[23] O. Beutel, R. Maraspini, K. Pombo-García, C. Martin-Lemaitre, and A. Honigmann, Cell **179**, 923 (2019), ISSN 00928674.

[24] M. Kar, F. Dar, T. J. Welsh, L. T. Vogel, R. Kühnemuth, A. Majumdar, G. Krainer, T. M. Franzmann, S. Alberti, C. A. M. Seidel, et al., Proceedings of the National Academy of Sciences **119**, e2202222119 (2022).

[25] P. Li, S. Banjade, H.-C. Cheng, S. Kim, B. Chen, L. Guo, M. Llaguno, J. V. Hollingsworth, D. S. King, S. F. Banani, et al., Nature **483**, 336 (2012), ISSN 1476-4687.

[26] T. M. Franzmann, M. Jahnel, A. Pozniakovsky, J. Mahamid, A. S. Holehouse, E. Nüske, D. Richter, W. Baumeister, S. W. Grill, R. V. Pappu, et al., Science (New York, N.Y.) **359**, eaao5654 (2018), ISSN 1095-9203.

[27] J. Guillén-Boixet, A. Kopach, A. S. Holehouse, S. Wittmann, M. Jahnel, R. Schlüßler, K. Kim, I. R. Trussina, J. Wang, D. Mateju, et al., Cell **181**, 346 (2020), ISSN 00928674.

[28] T. S. Harmon, A. S. Holehouse, M. K. Rosen, and R. V. Pappu, elife **6**, e30294 (2017).

[29] E. W. Martin, A. S. Holehouse, I. Peran, M. Farag, J. J. Incicco, A. Bremer, C. R. Grace, A. Soranno, R. V. Pappu, and T. Mittag, Science **367**, 694 (2020), ISSN 0036-8075, 1095-9203.

[30] U. Rana, C. P. Brangwynne, and A. Z. Panagiotopoulos, The Journal of Chemical Physics **155**, 125101 (2021), ISSN 0021-9606, 1089-7690.

[31] R. V. Pappu, S. R. Cohen, F. Dar, M. Farag, and M. Kar, Chemical Reviews p. acs.chemrev.2c00814 (2023), ISSN 0009-2665, 1520-6890.

[32] A. J. Bray and A. D. Rutenberg, Physical Review E **49**, R27 (1994).

[33] S. M. V, Z. Phys. Chem. **92**, 129 (1917).

[34] F. Oosawa and S. Asakura, *Thermodynamics of the Polymerization of Protein* (Academic Press, London ; New York, 1975), ISBN 978-0-12-527050-2.

[35] D. Blankschtein, G. M. Thurston, and G. B. Benedek, Physical Review Letters **54**, 955 (1985), ISSN 1079-7114.

[36] A. N. Semenov and M. Rubinstein, Macromolecules **31**, 1373 (1998), ISSN 0024-9297, 1520-5835.

[37] F. Tanaka, *Polymer Physics: Applications to Molecular Association and Thermoreversible Gelation* (Cambridge University Press, 2011), 1st ed., ISBN 978-0-7487-9497-3.

[38] D. Deviri and S. A. Safran, Soft Matter **16**, 5458 (2020), ISSN 1744-683X, 1744-6848.

[39] C. Weber, T. Michaels, and L. Mahadevan, eLife **8**, e42315 (2019), ISSN 2050-084X.

[40] T. C. T. Michaels, C. A. Weber, and L. Mahadevan, Proceedings of the National Academy of Sciences **116**, 14593 (2019).

[41] W. Pönisch, T. C. T. Michaels, and C. A. Weber, Biophysical Journal **122**, 197 (2023), ISSN 0006-3495.

[42] M. F. Hagan and F. Mohajerani, Preprint, Biophysics (2022).

[43] N. M. Kanaan, C. Hamel, T. Grabinski, and B. Combs, Nature Communications **11**, 2809 (2020), ISSN 2041-1723.

[44] S. Ray, N. Singh, R. Kumar, K. Patel, S. Pandey, D. Datta, J. Mahato, R. Panigrahi, A. Navalkar, S. Mehra, et al., Nature Chemistry **12**, 705 (2020), ISSN 1755-4349.

[45] I. Seim, A. E. Posey, W. T. Snead, B. M. Stormo, D. Klotsa, R. V. Pappu, and A. S. Gladfelter, Proceedings of the National Academy of Sciences **119**, e2120799119 (2022).

[46] P. J. Flory, The Journal of Chemical Physics **10**, 51 (1942).

[47] M. L. Huggins, Annals of the New York Academy of Sciences **43**, 1 (1942).

[48] S. A. Safran, *Statistical Thermodynamics of Surfaces, Interfaces, and Membranes* (CRC Press, Boca Raton, 2019), ISBN 978-0-429-49713-1.

[49] O. Adame-Arana, C. A. Weber, V. Zaburdaev, J. Prost, and F. Jülicher, Biophysical Journal **119**, 1590 (2020), ISSN 00063495.

[50] G. Bartolucci, O. Adame-Arana, X. Zhao, and C. A. Weber, Biophysical Journal **120**, 4682 (2021), ISSN 00063495.

[51] D. Bracha, M. T. Walls, M.-T. Wei, L. Zhu, M. Kurian, J. L. Avalos, J. E. Toettcher, and C. P. Brangwynne, Cell **175**, 1467 (2018), ISSN 00928674.

[52] D. M. Mitrea, C. R. Grace, M. Buljan, M.-K. Yun, N. J. Pytel, J. Satumba, A. Nourse, C.-G. Park, M. Madan Babu, S. W. White, et al., Proceedings of the National Academy of Sciences **111**, 4466 (2014), ISSN 0027-8424, 1091-6490.

[53] M. Feric, N. Vaidya, T. S. Harmon, D. M. Mitrea, L. Zhu, T. M. Richardson, R. W. Kriwacki, R. V. Pappu, and C. P. Brangwynne, Cell **165**, 1686 (2016), ISSN 0092-8674.

[54] F. Luo, X. Gui, H. Zhou, J. Gu, Y. Li, X. Liu, M. Zhao, D. Li, X. Li, and C. Liu, Nature Structural & Molecular Biology **25**, 341 (2018), ISSN 1545-9993, 1545-9985.

[55] L. Jawerth, E. Fischer-Friedrich, S. Saha, J. Wang, T. Franzmann, X. Zhang, J. Sachweh, M. Ruer, M. Ijavi, S. Saha, et al., Science **370**, 1317 (2020), ISSN 0036-8075, 1095-9203.

[56] J. Bauermann, S. Laha, P. M. McCall, F. Jülicher, and C. A. Weber, Journal of the American Chemical Society **144**, 19294 (2022), ISSN 0002-7863, 1520-5126.

[57] A. M. Miangolarra, A. Duperray-Susini, M. Coppey, and M. Castellana, Biophysical Journal **120**, 2394 (2021), ISSN 0006-3495.

[58] R. Milo and R. Phillips, *Cell Biology by the Numbers* (Garland Science, New York, 2015), ISBN 978-0-429-25877-0.

[59] A. Bar-Even, E. Noor, A. Flamholz, J. M. Buescher, and R. Milo, PLOS Computational Biology **7**, e1002166

(2011), ISSN 1553-7358.

[60] T. C. Michaels, A. Šarić, J. Habchi, S. Chia, G. Meisl, M. Vendruscolo, C. M. Dobson, and T. P. Knowles, Annual Review of Physical Chemistry **69**, 273 (2018).

[61] A. Patel, H. O. Lee, L. Jawerth, S. Maharana, M. Jahnel, M. Y. Hein, S. Stoynov, J. Mahamid, S. Saha, T. M. Franzmann, et al., Cell **162**, 1066 (2015), ISSN 00928674.

[62] M. Kato, T. W. Han, S. Xie, K. Shi, X. Du, L. C. Wu, H. Mirzaei, E. J. Goldsmith, J. Longgood, J. Pei, et al., Cell **149**, 753 (2012), ISSN 0092-8674.